Acta Mechanica Sinica (2012) 28(4):1068–1077
DOI 10.1007/s10409-012-0141-4

RESEARCH PAPER

Strong dependency of lithium diffusion on mechanical constraints in high-capacity Li-ion battery electrodes

Yi-Fan Gao · Min Zhou

Received: 17 April 2012 / Revised: 4 June 2012 / Accepted: 25 July 2012

Abstract The effect of external constraints on Li diffusion in high-capacity Li-ion battery electrodes is investigated using a coupled finite deformation theory. It is found that thin-film electrodes on rigid substrates experience much slower diffusion rates compared with free-standing films with the same material properties and geometric dimensions. More importantly, the study reveals that mechanical driving forces tend to retard diffusion in highly-constrained thin films when lithiation-induced softening is considered, in contrast to the fact that mechanical driving forces always enhance diffusion when deformation is fully elastic. The results provide further proof that nano-particles are a better design option for next-generation alloy-based electrodes compared with thin films.

Keywords Li-ion battery · Inelastic flow · Lithiation induced softening · Changing rate

1 Introduction

Negative electrodes based on amorphous lithium alloys have attracted significant interest because they offer capacities much higher than those of graphite electrodes [1]. However, when guest atoms are inserted into or extracted from these electrodes, the material expands or shrinks by up to ~300% [2], inducing stresses that can cause material cracking [3]. One way to mitigate the problem is to reduce the size of the electrodes. In particular, electrodes made of nano-sized structures such as nanowires (NWs), nanotubes and nanoscale core-shell structures have been shown to be particularly effective in avoiding fracture [4–8].

Besides higher capacity and better cyclability, faster operational charging rate is another important desideratum in battery design [9]. In order to shorten the charging time, it is essential to enhance transport kinetics by optimizing material properties and electrode geometries. It has been suggested that both surface transport and bulk diffusion of lithium are strongly coupled with the state of mechanical stress [3]. Bower et al. [10] developed a comprehensive framework and used it to analyze the time-dependent plasticity in thin-film Li/Si electrodes. Zhao et al. [11] considered plastic deformation and showed that inelastic flow can significantly alleviate stresses in Li/Si. Recent experiments by Soni et al. [12] suggest that the overall charging speed of Li/Si is more likely to be limited by diffusion inside the electrode rather than by surface transport, at least for thin films with thickness above 250 nm. However, it is not well understood how mechanical constraints affect the diffusion in alloy-based electrodes, especially when both two-way coupling and large deformation are present.

In this paper, we investigate the effect of external constraints on Li diffusion using a fully coupled, finite deformation framework. It is found that thin-film electrodes on rigid substrates suffer from much slower diffusion rates compared with free-standing films (or nano-flakes in some applications) with the same material properties and geometric dimensions. Of particular interest is the surprising finding that mechanical driving forces tend to retard diffusion in thin-film electrodes when lithiation-induced softening is considered. This is in sharp contrast to the fact that mechanical stresses always enhance diffusion when the deformation is in the elastic regime. The result provides further support for nano-particles as a better alternative to thin films as alloy-based electrode material.

2 Two-way coupling between diffusion and stress development

For the analysis here, the electrode is assumed to be com-

Y. F. Gao · M. Zhou (✉)
The George W. Woodruff School of Mechanical Engineering,
The School of Materials Science and Engineering,
Georgia Institute of Technology, Atlanta, GA30332-0405, USA
e-mail: min.zhou@gatech.edu

M. Zhou (✉)
WCU Program on Multiscale Mechanical Design,
School of Mechanical and Aerospace Engineering,
Seoul National University, Seoul, Korea

posed of two chemical species: host (denoted as H) and guest (lithium). Good electric conductance is assumed so that the whole electrode is at the same electric potential. During charge/discharge, lithium atoms diffuse in the electrode, while the host atoms are assumed to be immobile. It should be noted that Johari et al. [13] recently calculated the diffusivity of both Li and Si in silicon-based electrodes at room temperature and found that the ratio between Si and Li diffusivities in amorphous Li/Si falls into the range of 0.8×10^{-2}–1.39×10^{-2}. Although even such low values of host diffusivity $\left(D^{\mathrm{H}}\right)$ may have non-negligible effect on the evolution of stresses, we assume $D^{\mathrm{H}}=0$ here as a first-order approximation to simplify the analysis and focus on the effect of external constraints on Li transport. The conclusions thus drawn should apply to cases with finite values of D^{H} as long as it is much smaller than the diffusivity D^{Li} of Li.

Under the assumption of negligible host diffusivity, the host atoms can be treated as a scaffold through which Li transports. The movement of this scaffold defines the continuum deformation $\boldsymbol{x}=\boldsymbol{x}(\boldsymbol{X},t)$ during charge/discharge. The deformation of an infinitesimal volume element can then be characterized by the deformation gradient $\boldsymbol{F}=\partial\boldsymbol{x}/\partial\boldsymbol{X}$ with $F_{iJ}=\partial x_i/\partial X_J$. The Eulerian concentrations of the host and lithium, namely the atomic numbers per unit current volume, are denoted by c^{H} and c^{Li}, respectively. Their Lagrangian counter parts C^{H} and C^{Li} are related to c^{H} and c^{Li} through $C^{\mathrm{H}}=\det(\boldsymbol{F})\,c^{\mathrm{H}}$ and $C^{\mathrm{Li}}=\det(\boldsymbol{F})\,c^{\mathrm{Li}}$. Since host diffusion is neglected, C^{H} does not change with time, and a single dimensionless composition $\xi\equiv C^{\mathrm{Li}}/C^{\mathrm{H}}$ can be used to conveniently characterize the local charging state.

Following the standard theory of large deformation plasticity, a Lee-type decomposition [15] can be performed to the deformation gradient

$$\boldsymbol{F}=\boldsymbol{F}^{\mathrm{e}}\cdot\boldsymbol{F}^{\mathrm{SF}}\cdot\boldsymbol{F}^{\mathrm{p}}, \tag{1}$$

where $\boldsymbol{F}^{\mathrm{e}}$, $\boldsymbol{F}^{\mathrm{SF}}$ and $\boldsymbol{F}^{\mathrm{p}}$ are the elastic, stress-free volumetric and plastic deformation gradients, respectively [16, 17]. The velocity gradient is

$$\begin{aligned}L&=\dot{\boldsymbol{F}}\cdot\boldsymbol{F}^{-1}\\&=\dot{\boldsymbol{F}}^{\mathrm{e}}\cdot(\boldsymbol{F}^{\mathrm{e}})^{-1}+\boldsymbol{F}^{\mathrm{e}}\cdot\dot{\boldsymbol{F}}^{\mathrm{SF}}\cdot\left(\boldsymbol{F}^{\mathrm{SF}}\right)^{-1}\cdot(\boldsymbol{F}^{\mathrm{e}})^{-1}\\&\quad+\boldsymbol{F}^{\mathrm{e}}\cdot\boldsymbol{F}^{\mathrm{SF}}\cdot\dot{\boldsymbol{F}}^{\mathrm{p}}\cdot(\boldsymbol{F}^{\mathrm{p}})^{-1}\cdot\left(\boldsymbol{F}^{\mathrm{SF}}\right)^{-1}\cdot(\boldsymbol{F}^{\mathrm{e}})^{-1},\end{aligned} \tag{2}$$

and the associated rates of deformation are

$$\begin{aligned}\boldsymbol{D}^{\mathrm{e}}&\equiv\left[\dot{\boldsymbol{F}}^{\mathrm{e}}(\boldsymbol{F}^{\mathrm{e}})^{-1}\right]_{\mathrm{sym}},\\\boldsymbol{D}^{\mathrm{SF}}&\equiv\left[\boldsymbol{F}^{\mathrm{e}}\cdot\dot{\boldsymbol{F}}^{\mathrm{SF}}\cdot\left(\boldsymbol{F}^{\mathrm{SF}}\right)^{-1}\cdot(\boldsymbol{F}^{\mathrm{e}})^{-1}\right]_{\mathrm{sym}},\\\boldsymbol{D}^{\mathrm{p}}&\equiv\left[\boldsymbol{F}^{\mathrm{e}}\cdot\boldsymbol{F}^{\mathrm{SF}}\cdot\dot{\boldsymbol{F}}^{\mathrm{p}}\cdot(\boldsymbol{F}^{\mathrm{p}})^{-1}\cdot\left(\boldsymbol{F}^{\mathrm{SF}}\right)^{-1}\cdot(\boldsymbol{F}^{\mathrm{e}})^{-1}\right]_{\mathrm{sym}},\\\boldsymbol{D}&\equiv[\boldsymbol{L}]_{\mathrm{sym}}=\boldsymbol{D}^{\mathrm{e}}+\boldsymbol{D}^{\mathrm{SF}}+\boldsymbol{D}^{\mathrm{p}}.\end{aligned} \tag{3}$$

In this paper, we assume the stress-free expansion due to concentration change is isotropic so that

$$\boldsymbol{F}^{\mathrm{SF}}=\left[J^{\mathrm{SF}}\left(C^{\mathrm{Li}}\right)\right]^{1/3}\boldsymbol{I}, \tag{4}$$

where $J^{\mathrm{SF}}\left(C^{\mathrm{Li}}\right)=\det\left(\boldsymbol{F}^{\mathrm{SF}}\right)$ measures the volume change due to changes in Li concentration. On the other hand, the elastic strain associated with $\boldsymbol{F}^{\mathrm{e}}$ is

$$\boldsymbol{\varepsilon}^{\mathrm{e}}\equiv\frac{1}{2}\left[(\boldsymbol{F}^{\mathrm{e}})^{\mathrm{T}}\boldsymbol{F}^{\mathrm{e}}-\boldsymbol{I}\right]. \tag{5}$$

We assume small $\boldsymbol{\varepsilon}^{\mathrm{e}}$, i.e., the elastic stretch $\boldsymbol{U}^{\mathrm{e}}$ associated with $\boldsymbol{F}^{\mathrm{e}}=\boldsymbol{R}^{\mathrm{e}}\boldsymbol{U}^{\mathrm{e}}$ is small although the rotation $\boldsymbol{R}^{\mathrm{e}}$ may be finite. The Cauchy stress $\boldsymbol{\sigma}$ is given by

$$\sigma_{ij}=F^{\mathrm{e}}_{iK}\left(3K\varepsilon^{\mathrm{e}}_{m}\delta_{KL}+2G\varepsilon^{e'}_{KL}\right)F^{\mathrm{e}}_{jL}, \tag{6}$$

where $\varepsilon^{\mathrm{e}}_{m}\equiv\varepsilon^{\mathrm{e}}_{kk}/3$ and $\varepsilon^{e'}_{ij}\equiv\varepsilon^{\mathrm{e}}_{ij}-\varepsilon^{\mathrm{e}}_{m}\delta_{ij}$ are the isotropic and deviatoric parts of the elastic strain; K and G are the bulk and shear modulus, respectively. The particular form of Eq. (6) ensures that the correct rotational relationship between $\boldsymbol{\varepsilon}^{\mathrm{e}}$ and $\boldsymbol{\sigma}$ is maintained.

Plastic deformation is assumed to follow the associated flow rule with composition-dependent yield surface $\sigma_{\mathrm{Y}}=\sigma_{\mathrm{Y}}\left(C^{\mathrm{Li}}\right)$ in the form of

$$Q=Q(\boldsymbol{\sigma})=\frac{1}{2}\boldsymbol{\sigma}^{\mathrm{dev}}:\boldsymbol{\sigma}^{\mathrm{dev}}-\frac{1}{3}\sigma_{\mathrm{Y}}^{2}=0, \tag{7}$$

where $\boldsymbol{\sigma}^{\mathrm{dev}}\equiv\boldsymbol{\sigma}-\mathrm{tr}(\boldsymbol{\sigma})/3\boldsymbol{I}$ is the deviatoric part of the Cauchy stress. Below the yielding threshold, $\boldsymbol{D}$ is simply given by the rate form of Eqs. (4) and (6), i.e.

$$\boldsymbol{D}=\left(\frac{1}{9K}-\frac{1}{6G}\right)\mathrm{tr}\left(\mathring{\boldsymbol{\sigma}}\right)\boldsymbol{I}+\frac{\mathring{\boldsymbol{\sigma}}}{2G}+\left[\frac{1}{3}\frac{\partial\left(\ln J^{\mathrm{SF}}\right)}{\partial C^{\mathrm{Li}}}\dot{C}^{\mathrm{Li}}\right]\boldsymbol{I}. \tag{8}$$

Here, $\mathring{\boldsymbol{\sigma}}\equiv\dot{\boldsymbol{\sigma}}-\boldsymbol{W}\cdot\boldsymbol{\sigma}+\boldsymbol{\sigma}\cdot\boldsymbol{W}$ is the Jaumann objective rate of $\boldsymbol{\sigma}$, with $\boldsymbol{W}=\left(\boldsymbol{L}-\boldsymbol{L}^{\mathrm{T}}\right)/2$ being the spin tensor. Upon yielding, the rate of deformation including plasticity is

$$\begin{aligned}\boldsymbol{D}&=\left(\frac{1}{9K}-\frac{1}{6G}\right)\mathrm{tr}\left(\mathring{\boldsymbol{\sigma}}\right)\boldsymbol{I}+\frac{\mathring{\boldsymbol{\sigma}}}{2G}\\&\quad+\left[\frac{1}{3}\frac{\partial\left(\ln J^{\mathrm{SF}}\right)}{\partial C^{\mathrm{Li}}}\dot{C}^{\mathrm{Li}}\right]\boldsymbol{I}+\dot{\lambda}\frac{\partial Q}{\partial\boldsymbol{\sigma}},\end{aligned} \tag{9}$$

where the scalar rate $\dot{\lambda}$ can be determined from consistency conditions and takes the form of

$$\dot{\lambda}=\frac{3}{2}\frac{1}{\sigma_{\mathrm{Y}}^{2}}\boldsymbol{D}:\boldsymbol{\sigma}^{\mathrm{dev}}+\frac{\dot{C}^{\mathrm{Li}}}{2G\sigma_{\mathrm{Y}}}\frac{\partial\sigma_{\mathrm{Y}}}{\partial C^{\mathrm{Li}}}. \tag{10}$$

Equations (9) and (10) give the mechanical constitutive behavior when the yield stress is reached, while Eq. (8) governs the deformation in the elastic regime. Together with the conservation of momentum equation

$$\frac{\partial\sigma_{ji}}{\partial x_j}=0, \tag{11}$$

the above equations allow the deformation of the electrode material to be determined.

The diffusive flux of lithium can be measured either in the Lagrangian frame as $\boldsymbol{J}^{\mathrm{Li}}$ or in the updated Lagrangian frame as $\boldsymbol{j}^{\mathrm{Li}}$. These measure are related through $\boldsymbol{f} \equiv \boldsymbol{F}^{-1}$ as

$$J_K^{\mathrm{Li}} = \det(\boldsymbol{F})\, f_{Ki} j_i^{\mathrm{Li}}. \tag{12}$$

On one hand, $\boldsymbol{J}^{\mathrm{Li}}$ must satisfy the requirement of mass conservation such that

$$\frac{\partial C^{\mathrm{Li}}}{\partial t} + \frac{\partial J_K^{\mathrm{Li}}}{\partial X_K} = R_{\mathrm{b}}^{\mathrm{Li}}, \tag{13}$$

where $R_{\mathrm{b}}^{\mathrm{Li}}$ is the body source of Li measured in the Lagrangian frame. In this paper, we assume $R_{\mathrm{b}}^{\mathrm{Li}} = 0$. On the other hand, the Fick's law requires

$$J_K^{\mathrm{Li}} = -\frac{D^{\mathrm{Li}}}{k_{\mathrm{B}}\theta} f_{Ki} f_{Ji} C^{\mathrm{Li}} \frac{\partial \mu^{\mathrm{Li}}}{\partial X_J}, \tag{14}$$

where $D^{\mathrm{Li}} = D^{\mathrm{Li}}(\xi)$ is the composition-dependent diffusivity of lithium, k_{B} is the Boltzmann constant; θ is the temperature, and μ^{Li} is the chemical potential of lithium which can be expressed as

$$\mu^{\mathrm{Li}} = \mu_{\mathrm{SF}}^{\mathrm{Li}} - \det(\boldsymbol{F}^{\mathrm{e}})\, \Omega^{\mathrm{Li(SF)}} \sigma_m. \tag{15}$$

Here, $\sigma_m \equiv \sigma_{kk}/3$ is the hydrostatic stress, $\Omega^{\mathrm{Li(SF)}} \equiv \partial J^{\mathrm{SF}}/\partial C^{\mathrm{Li}}$ is the stress-free partial atomic volume of lithium, and $\mu_{\mathrm{SF}}^{\mathrm{Li}} = \mu_{\mathrm{SF}}^{\mathrm{Li}}(C^{\mathrm{Li}})$ is the isothermal chemical potential of lithium when the material is stress-free. Generally speaking, $\mu_{\mathrm{SF}}^{\mathrm{Li}}(C^{\mathrm{Li}})$ can be determined by fitting the activity coefficient to experimental open circuit potential (OCP) data [3]. To simplify the problem, however, we adopt the ideal-solution form of $\mu_{\mathrm{SF}}^{\mathrm{Li}}$ originally proposed by Larche and Cahn [18] and subsequently used by Purkayastha and McMeeking [19] and Yang et al. [20] in the form of

$$\mu_{\mathrm{SF}}^{\mathrm{Li}} = \mu_*^{\mathrm{Li}} + k\theta \ln \frac{\xi}{\xi_{\max} - \xi}, \tag{16}$$

where $\xi_{\max}$ is the maximum charging limit of the electrode material and the constant μ_*^{Li} is a reference chemical potential. The composition-dependent diffusivity D^{Li}, on the other hand, is taken to be [19, 20]

$$D^{\mathrm{Li}} = D_0^{\mathrm{Li}}(1 - \xi/\xi_{\max}) = D_0^{\mathrm{Li}}\left(1 - C^{\mathrm{Li}}/C_{\max}^{\mathrm{Li}}\right). \tag{17}$$

Combining Eqs. (14) and (17) leads to the lithium flux of

$$\begin{aligned} J_K^{\mathrm{Li}} &= J_K^{\mathrm{Li,chem}} + J_K^{\mathrm{Li,mech}}, \\ J_K^{\mathrm{Li,chem}} &= -D_0^{\mathrm{Li}} f_{Ki} f_{Ji} \tfrac{\partial C^{\mathrm{Li}}}{\partial X_J}, \\ J_K^{\mathrm{Li,mech}} &= \frac{D_0^{\mathrm{Li}}\left(1 - C^{\mathrm{Li}}/C_{\max}^{\mathrm{Li}}\right)}{k_{\mathrm{B}}\theta} f_{Ki} f_{Ji} C^{\mathrm{Li}} \frac{\partial\left(\Omega^{\mathrm{Li(SF)}}\sigma_m\right)}{\partial X_J}. \end{aligned} \tag{18}$$

In the above relations, $J_K^{\mathrm{Li,chem}}$ and $J_K^{\mathrm{Li,mech}}$ are contributions due to chemical interaction and mechanical driving force, respectively. According to Purkayastha and McMeeking [19], the main advantage of Eqs. (16) and (17) is that it correctly captures the fact that the stress-gradient-driven diffusion flux $J_K^{\mathrm{Li,mech}}$ (cf. Eq. (18)) vanishes at the charging limits of $\xi = 0$ and $\xi = \xi_{\max}$.

One of the major numerical challenges here is associated with the gradient of the hydrostatic stress (i.e. $\partial\sigma_m/\partial X_J$) that appears in Eq. (18) when a finite element (FE) method is used. Since $\partial\sigma_m/\partial X_J \propto \partial\varepsilon_m^{\mathrm{e}}/\partial X_J$, either the strain gradient or the stress gradient itself has to be calculated numerically. We used the mixed finite element method [14] to handle this issue when analyzing coupled diffusion/deformation processes. This method not only uses the deformation and host/guest concentrations as nodal variables, but also interpolates σ_m as a redundant degree of freedom, thereby automatically resolving $\partial\sigma_m/\partial X_J$ required. The details of this numerical framework will not be elaborated in this paper.

3 Numerical results and discussion

The rate-form, large-deformation, mixed finite element framework is used to analyze the two-way coupling between diffusion and stress development. The issues of focus are

(1) how does the stress-gradient-driven diffusion flux $J_K^{\mathrm{Li,mech}}$ affect the transport of Li under different mechanical constraints and

(2) as an important figure of merit for batteries, how significantly does this difference affect the operational charging rate?

To this end, we consider two simple electrode configurations with essentially the same material properties and geometric setup, but different mechanical constraints. The first configuration (Fig. 1a) involves a thin film of $\mathrm{Li}_\xi\mathrm{Si}$ (host is Si) with thickness H perfectly bonded to a substrate which has a stiffness much higher than that of the film and, therefore, can be treated as rigid. A constant influx of Li is specified at the top surface so that the electrode is charged under galvanostatic conditions. This surface influx is measured in the reference configuration as

$$J_{\mathrm{Surf}}^{\mathrm{Li}} = -J_Z^{\mathrm{Li}}(H) = \frac{H\xi_{\max}C^{\mathrm{Si}}}{T_0}, \tag{19}$$

where T_0 is the nominal time for achieving full charge. Here, we take $T_0 = 4$ h (1/4 C charging).

The second configuration (Fig. 1b) has the same thickness and influx, but the bottom surface is only constrained in the z-direction and is free to move in the other directions. This is equivalent to a film with a thickness of $2H$ and the same influx on both faces. Understandably, the two configurations will develop very different stresses due to the different constraints. Our goal is to analyze how $C^{\mathrm{Li}}(Z,t)$ is distributed (Z denotes the Lagrangian coordinate) with two-way deformation-diffusion coupling under different mechanical constraints.

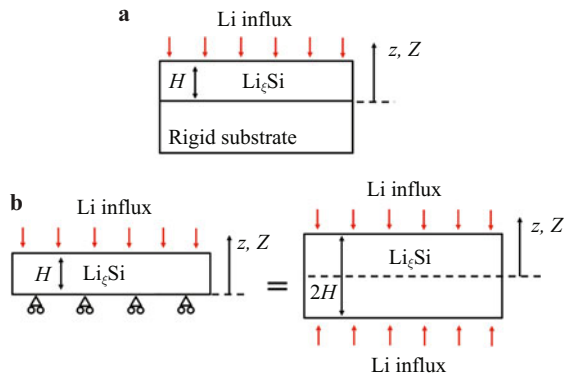

Fig. 1 The two configurations used to analyze how mechanical constraints affect Li transport. **a** Thin film with thickness H perfectly bonded to a rigid substrate. A galvanostatic influx is prescribed on the top surface; **b** A thin film which is constrained only in the z-direction at the bottom (due to symmetry) with the same galvanostatic influx at the top face (left). This configuration is equivalent to a film with a thickness of $2H$ under symmetric influxes from both faces (right). The coordinate in the current configuration is denoted as z and the coordinate in the Lagrangian configuration is denoted as Z

The material properties are $\Omega^{\mathrm{Li(SF)}} = 14.2 \times 10^{-3}$ nm^3 [21, 22], $D_0^{\mathrm{Li}} = 10^{-12}$ cm^{2}s^{-1}, $\xi_{\max} = 3.75$ and $C^{\mathrm{Si}} = C_0^{\mathrm{Si}} = 49.3$ nm^{-3}. The temperature is taken to be 300 K. A calculation is first carried out with a composition-independent Young's modulus value of $E = 80$ GPa, Poission's ratio value of $\nu = 0.22$ and yield stress value of $\sigma_{\mathrm{Y}} = 1.75$ GPa. The corresponding bulk modulus K and shear modulus G are 47.62 GPa and 32.79 GPa, respectively. This calculation is used as the baseline case to study the effect of lithiation-induced softening on Li diffusion. The second calculation involves composition-dependent bulk modulus $K = (12.46\xi + 65.44)/(1 + \xi)$ GPa, shear modulus of $G = (7.63\xi + 35.51)/(1 + \xi)$ GPa [23], and yield stress of $\sigma_{\mathrm{Y}} = (1.75 + 0.167\xi)\,/\,(1 + \xi)$ GPa, allowing comparison with the baseline case to be made. The variation of yield stress with concentration represents a simple interpolation between $\sigma_{\mathrm{Y}} = 1.75$ GPa at $\xi = 0$ and $\sigma_{\mathrm{Y}} = 0.5$ GPa at $\xi = \xi_{\max}$ [24, 25] using the rule of mixture.

3.1 Stress-enhanced diffusion during elastic deformation (configuration b)

Figure 2 shows the profiles of normalized lithium concentration ξ and the stresses in a film with a thickness of $H = 500$ nm and constraint only in the z-direction at the bottom (configuration Fig. 1b). When $J_K^{\mathrm{Li,mech}}$ is neglected, the concentration builds up in the early stages of charging (Fig. 2a), accompanied by increases in the in-plane stresses (Fig. 2c). As stresses increase, the surface and center of the film reach the yield threshold and begin to flow plastically, leading to plateaus in the stress profiles at $t = (0.012\,5\text{–}0.1)T_0$. The time scale for this transient build up of concentration is $\tau^{\mathrm{Li}} \sim H^2/4D_0^{\mathrm{Li}} \sim 6 \times 10^2$ s. Beyond τ^{Li}, the long-term profile of ξ continues to evolve, albeit slowly; however this evolution is no longer due to transient effects. In Fig. 2d, the concentration profiles that account for the effects of $J_K^{\mathrm{Li,mech}}$ show similar behavior in early stages as those in Fig. 2a, but reflect more uniform distribution of Li as time progresses. Also, the stress levels are much lower (Fig. 2f) compared with the case without the effect of $J_K^{\mathrm{Li,mech}}$ (Fig. 2c). In fact, the reduction in stresses is so significant that the yield threshold is never reached in Fig. 2f, as a result the deformation is fully within the elastic regime throughout the charging process. A simple analysis shows that when $J_K^{\mathrm{Li,mech}}$ is considered, the diffusion is no-longer governed by D_0^{Li} itself. Instead, J_Z^{Li} is governed by an effective diffusivity $D^{\mathrm{Li,eff}}$ such that [26–28]

$$J_Z^{\mathrm{Li}} = -D^{\mathrm{Li,eff}} f_{Ki} f_{Ji} \frac{\partial C^{\mathrm{Li}}}{\partial Z}$$
$$\text{where } D^{\mathrm{Li,eff}} \equiv D_0^{\mathrm{Li}} + D^{\mathrm{Li,mech}} \text{ and} \tag{20}$$
$$D^{\mathrm{Li,mech}} = \frac{C^{\mathrm{Li}}\left(1 - C^{\mathrm{Li}}/C_{\max}^{\mathrm{Li}}\right)}{k_{\mathrm{B}}\theta} \frac{(\Omega^{\mathrm{G(SF)}})^2}{J^{\mathrm{SF}}} \frac{2ED_0^{\mathrm{Li}}}{9\,(1-\nu)}.$$

This relationship is valid as long as the deformation is fully elastic. Here, the second term (i.e. $D^{\mathrm{Li,mech}}$) in the expression of $D^{\mathrm{Li,eff}}$ is always positive. It is due to the mechanical driving force for diffusion and is ~20 times larger than D_0^{Li} at $\xi/\xi_{\max} = 0.5$. This effect leads to much faster lithium transport due to the fact that stresses always try to "squeeze" Li from compressed regions into tensile regions, hence the name stress-enhanced diffusion (SED) [26]. It should be noted that classical theories of diffusion suggest an asymptotic shape of concentration profile which remains unchanged once $t \gg \tau^{\mathrm{Li}}$. Here, however, the long-term shapes of the concentration and stress profiles continue to evolve even for $t \gg \tau^{\mathrm{Li}}$. Two mechanisms are responsible. The first is associated with the fact that $D^{\mathrm{Li,eff}} = D^{\mathrm{Li,eff}}(C^{\mathrm{Li}})$ is concentration-dependent [cf. Eq. (20)]. Since $D^{\mathrm{Li,mech}} \propto C^{\mathrm{Li}}(1 - C^{\mathrm{Li}}/C_{\max}^{\mathrm{Li}})$, SED is less pronounced when ξ is close 0 or $\xi_{\max}$. Therefore the concentration profiles are steeper at the end of charging process ($t = 0.952T_0$) than at $t = 0.1T_0$ in Fig. 2e. By the same token, the stresses are also higher at the end than at $t = 0.1\ T_0$. This first mechanism is relevant only for the situation when $J_K^{\mathrm{Li,mech}}$ is considered. The second mechanism, which is relevant with or without $J_K^{\mathrm{Li,mech}}$, is associated with the geometric non-linearity under finite deformations (Eq. (28)). This mechanism will be discussed later.

When $J_K^{\mathrm{Li,mech}}$ is neglected, the Li concentration reaches its fully-charged limit of $\xi_{\max}$ on the surface at $t = 0.864\ T_0$, rendering further galvanostatic charging practically impossible. In experiments, the charging condition

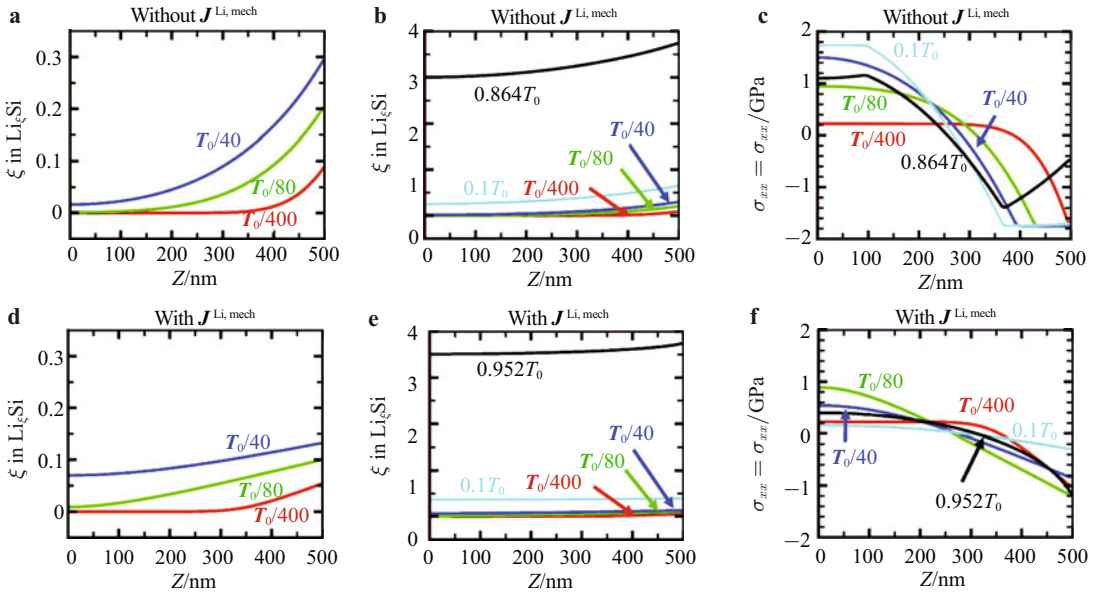

Fig. 2 **a, b, d, e** Normalized Li concentration and **c, f** stress profiles in a film with a thickness of $H = 500$ nm and constraint only in the z-direction at the bottom (configuration in Fig. 1b). **a-c** Normalized concentration and stress profiles when the mechanical driving force for diffusion is not considered. **d-f** Normalized concentration and stress profiles when the mechanical driving force for diffusion is considered. For clarity, **a** and **d** show, with a finer vertical axis scale, the three early-stage profiles in **b** and **e**, respectively

is usually switched to potential-static at this point so that $\xi = \xi_{\max}$ is maintained on the surface while ξ in the interior further increases. This charging regimen is not considered in the simulations here. Instead, the simulations are stopped once the surface concentration ξ reaches $\xi_{\max}$ and the average Li concentration $\bar{\xi}_{\text{end}}$ in the electrode at that point is used for comparison. This average value is directly related to the actual change time t_{end} via $\bar{\xi}_{\text{end}} = \xi_{\max} t_{\text{end}}/T_0$. Since the actual charging time t_{end} is always smaller than the nominal charging time T_0, $\bar{\xi}_{\text{end}}$ is always smaller than $\xi_{\max}$. Obviously, $\bar{\xi}_{\text{end}}$ depends on the charging rate which is controlled by $J^{\text{Li}}_{\text{Surf}}$. Higher charging rates lead to lower $\bar{\xi}_{\text{end}}$. To achieve the same $\bar{\xi}_{\text{end}}$ through slower Li transport, lower operational charging rate must be used. Calculations show that, for the material conditions analyzed under the nominal changing rate of $T_0 = 4$ h, $\bar{\xi}_{\text{end}} = 0.952\xi_{\max}$ when $J^{\text{Li,mech}}_K$ is considered and, in contrast, $\bar{\xi}_{\text{end}} = 0.864\xi_{\max}$ when $J^{\text{Li,mech}}_K$ is neglected. Clearly, the SED effect (stress contribution to diffusion) not only lowers stresses but also increases allowable operational charging rate through enhanced Li transport (and, therefore, more uniform Li distribution). This effect will be further analyzed later in the context of different mechanical constraints.

A look at the distribution of lithium fluxes also provides insights. Figure 3 shows the Lagrangian lithium fluxes as normalized by the surface influx (Eq. (19)). Only J^{Li}_Z is plotted because $J^{\text{Li}}_X = J^{\text{Li}}_Y = 0$ due to symmetry. For both the situations with and without the effect of $J^{\text{Li,mech}}$, $J^{\text{Li}}_Z = -J^{\text{Li}}_{\text{Surf}}$ at the surface ($Z = 500$ nm) and $J^{\text{Li}}_Z = 0$ at the center ($Z = 0$ nm). Since the problem is 1-D here, the conservation of mass (Eq. (13)) requires

$$J^{\text{Li}}_Z(Z) = J^{\text{Li}}_Z(0) - \int_0^Z \frac{\partial C^{\text{Li}}}{\partial t}\mathrm{d}Z = -C^{\text{Si}}\int_0^Z \frac{\partial \xi}{\partial t}\mathrm{d}Z. \tag{21}$$

The normalized concentration $\xi \equiv C^{\text{Li}}/C^{\text{Si}}$ can be decomposed into two parts: the average Li-concentration part

$$\bar{\xi} \equiv \frac{1}{H}\int_0^H \xi \mathrm{d}Z, \tag{22}$$

and the inhomogeneity part

$$\Delta\xi \equiv \xi - \bar{\xi}. \tag{23}$$

By Eqs. (22), (21) and (19),

$$\bar{\xi} = \frac{t}{T_0}\xi_{\max}. \tag{24}$$

Therefore, Eqs. (21)–(24) require

$$J^{\text{Li}}_Z(Z) = -\frac{Z}{H}J^{\text{Li}}_{\text{Surf}} - C^{\text{Si}}\int_0^Z \frac{\partial \Delta\xi}{\partial t}\mathrm{d}Z. \tag{25}$$

Since $\int_0^0 (\partial\Delta\xi/\partial t)\,\mathrm{d}Z = \int_0^{\mathrm{H}} (\partial\Delta\xi/\partial t)\,\mathrm{d}Z = 0$, Eq. (25) has a Taylor-expansion in the form of

$$J^{\text{Li}}_Z(Z,t) = -\frac{Z}{H}J^{\text{Li}}_{\text{Surf}} - \frac{Z}{H}\sum_{n=1}^{\infty}\left(1-\frac{Z}{H}\right)^n J^{\text{Li}(n)}_Z(t) \tag{26}$$

where the coefficients $J^{\text{Li}(n)}_Z(t)$ are directly related to the time rate $\partial\Delta\xi/\partial t$ of the concentration inhomogeneity.

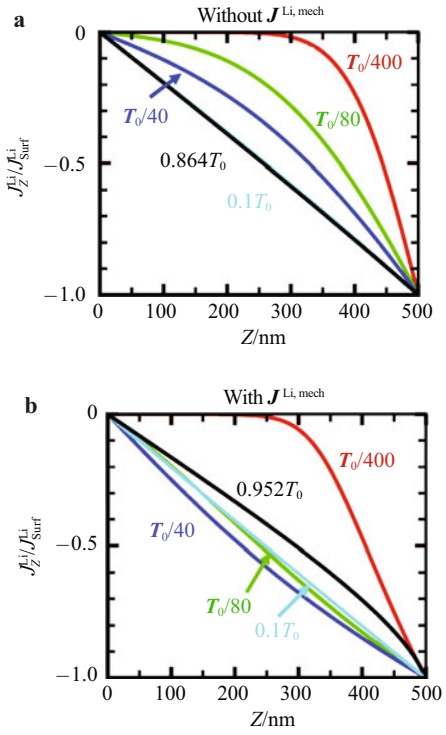

Fig. 3 Lagrangian lithium flux normalized by surface influx with **a** mechanical driving force not considered and **b** mechanical driving force considered. Z denotes Lagrangian coordinate. The film is constrained only in the z-direction at the bottom and lithiation-induced softening is not considered

For the case in which $\boldsymbol{J}^{\text{Li,mech}}$ is not considered (Fig. 3a), $\partial\Delta\xi/\partial t = 0$ once the transient build-up of ξ has completed ($t > \tau^{\text{Li}}$). Consequently, $J_Z^{\text{Li}(n)}(t) = 0$ except for the initial transient stages, explaining why the $J_Z^{\text{Li}}(Z)$ profiles in Fig. 3a are linear for $t = 0.1T_0$ and $0.864T_0$. For the case in which $J^{\text{Li,mech}}$ is considered, the effective diffusivity $D^{\text{Li,eff}}$ (Eq. (20)) changes slowly even after the initial transient development finishes. This long-term modulation of $D^{\text{Li,eff}}$ leads to non-zero $\partial\Delta\xi/\partial t$ and hence non-zero $J_Z^{\text{Li}(n)}(t)$. As a result, the $J_Z^{\text{Li}}(Z)$ profiles at $t = 0.1T_0$ and $t = 0.952T_0$ deviate from the $J_Z^{\text{Li}} = -ZJ_{\text{Surf}}^{\text{Li}}/H$ line, as seen in Fig. 3b. Such a deviation is nevertheless fairly small and a first-order approximation of

$$J_Z^{\text{Li}} \approx -\frac{Z}{H} J_{\text{Surf}}^{\text{Li}} \,. \tag{27}$$

can lead to some interesting observations. Specifically, when the thin film is constrained only in the z-direction (Fig. 1b), the deformation gradient is approximately (in the elastic regime $\boldsymbol{F}^{\text{p}} = \boldsymbol{I}$)

$$\boldsymbol{F} \approx \boldsymbol{F}^{\text{p}}\boldsymbol{F}^{\text{SF}} = \left(J^{\text{SF}}\right)^{1/3} \begin{pmatrix} 1 & 0 & 0 \\ 0 & 1 & 0 \\ 0 & 0 & 1 \end{pmatrix}. \tag{28}$$

Under this deformation, the concentration gradient $\partial\xi/\partial Z$ can be determined from Eqs. (18), (20) and (27) to be

$$\frac{\partial C^{\text{Li}}}{\partial Z} = C^{\text{Si}}\frac{\partial \xi}{\partial Z} \approx \frac{\left(J^{\text{SF}}\right)^{2/3} Z J_{\text{Surf}}^{\text{Li}}}{D^{\text{Li,eff}} H}. \tag{29}$$

By the same token, $\partial\xi/\partial Z$ without the effect of $\boldsymbol{J}^{\text{Li,mech}}$ is governed by

$$\frac{\partial C^{\text{Li}}}{\partial Z} = C^{\text{Si}}\frac{\partial \xi}{\partial Z} \approx \frac{\left(J^{\text{SF}}\right)^{2/3} Z J_{\text{Surf}}^{\text{Li}}}{D_0^{\text{Li}} H}. \tag{30}$$

Equations (29) and (30) show that the shapes of the long-term ξ profiles are approximately quadratic as long as the transient build-up stages have finished, regardless of if $\boldsymbol{J}^{\text{Li,mech}}$ is considered or not. Moreover, when $\boldsymbol{J}^{\text{Li,mech}}$ is not accounted for, the diffusion is controlled by a constant diffusivity D_0^{Li}. Because J^{SF} is larger at higher ξ, the concentration inhomogeneity $\Delta\xi$ increases with t according to Eq. (30). This is why the Li concentration profile is steeper at $t = 0.863T_0$ than at $t = 0.1T_0$ in Fig. 2b. Such a long-term evolution of ξ profile (Fig. 2b) is fundamentally different from that seen in Fig. 2e: although the geometric effect is also present in Fig. 2e, the evolution of ξ profile in Fig. 2e is instead mainly due to the slow change of $D^{\text{Li,eff}}$.

The finite dimensional change (Eq. (28)) is also responsible for the observation that the stresses at $t = 0.864T_0$ are lower than those at $0.1T_0$ in Fig. 2c. The analysis by Gao and Zhou [26] shows that, under fully elastic conditions, stresses scale with the current dimensions according to

$$\boldsymbol{\sigma} \propto \Delta\xi/\boldsymbol{J}^{\text{SF}}. \tag{31}$$

On the other hand, Eq. (30) indicates that $\Delta\xi \propto (\boldsymbol{J}^{\text{SF}})^{2/3}/D_0^{\text{Li}}$. Therefore,

$$\boldsymbol{\sigma} \propto \left(\boldsymbol{J}^{\text{SF}}\right)^{-1/3}/D_0^{\text{Li}} \tag{32}$$

When $J^{\text{Li,mech}}$ is not considered, the diffusivity D_0^{Li} is constant and Eq. (32) indicates that stresses are lower when J^{SF} is higher. This explains why the stresses at $t = 0.864T_0$ are lower than those at $0.1T_0$, as seen in Fig. 2c. This geometric effect on long-term stresses is so significant that the plastic regions in Fig. 2c are unloaded back to the elastic regime as charging proceeds and the associated residue plastic strain leads to the positive slopes of $\sigma_{xx} = \sigma_{yy}$ at the center and surface at $t = 0.864T_0$.

It should be noted that the approximation embodied in Eq. (28) is, strictly speaking, valid only when the deformation is elastic throughout the charging history, while the deformation in Fig. 2c does involve plasticity. Nevertheless, the above analysis qualitatively explains the long-term evolution of concentration and stress profiles in Fig. 2c because most of the charging history is in the elastic regime. It will be shown later that when the material undergoes full-scale yielding, Eq. (28) must be revised, and the associated finite deformation would result in very different concentration profiles, with or without $\boldsymbol{J}^{\text{Li,mech}}$.

3.2 Neutralization of SED due to plastic flow (configuration a)

The diffusion characteristics are drastically different when the thin film is fully constrained at the bottom, as shown in Fig. 4. First and foremost, due to the strong mechanical constraint, the film quickly reaches full-scale yielding regardless of if two-way coupling is accounted for (see Fig. 4c and 4f). More importantly, diffusive transport is much slower compared with that seen in Fig. 2. Specifically, $\bar{\xi}_{\text{end}} = 0.568\xi_{\max}$ without $J_K^{\text{Li,mech}}$ and $\bar{\xi}_{\text{end}} = 0.590\xi_{\max}$ with $J_K^{\text{Li,mech}}$. This occurs because of two reasons. First, when the material undergoes full-scale yielding, stress gradient essentially vanishes (specifically, $\nabla\sigma_m = 0$). Since $\left|J^{\text{Li,mech}}\right| \propto |\nabla\sigma_m|$, the absence of stress gradient removes the SED effect. Indeed, the fact that $\bar{\xi}_{\text{end}}$ is approximately the same with and without $J_K^{\text{Li,mech}}$ is a direct result of the loss of SED. A look at Fig. 4d reveals sudden changes in the slope of ξ profiles at the boundary between the elastic and plastic zones. The steeper slope in the plastic zone (surface side) indicates that the effective diffusivity in the yielded region is much lower than that in the elastic region. As the charging proceeds, the boundary between the two zones moves from the surface towards the interior. Once the boundary reaches the bottom, the whole electrode is plastic with low effective diffusivity. The second reason for the slower Li transport is different finite dimensional change. When the film is fully constrained by the substrate, deformation occurs only in the z-direction (normal to the film plane), and the deformation gradient is approximately

$$\boldsymbol{F} \approx \boldsymbol{F}^{\text{p}}\boldsymbol{F}^{\text{SF}} = \begin{pmatrix} 1 & 0 & 0 \\ 0 & 1 & 0 \\ 0 & 0 & J^{\text{SF}} \end{pmatrix}. \tag{33}$$

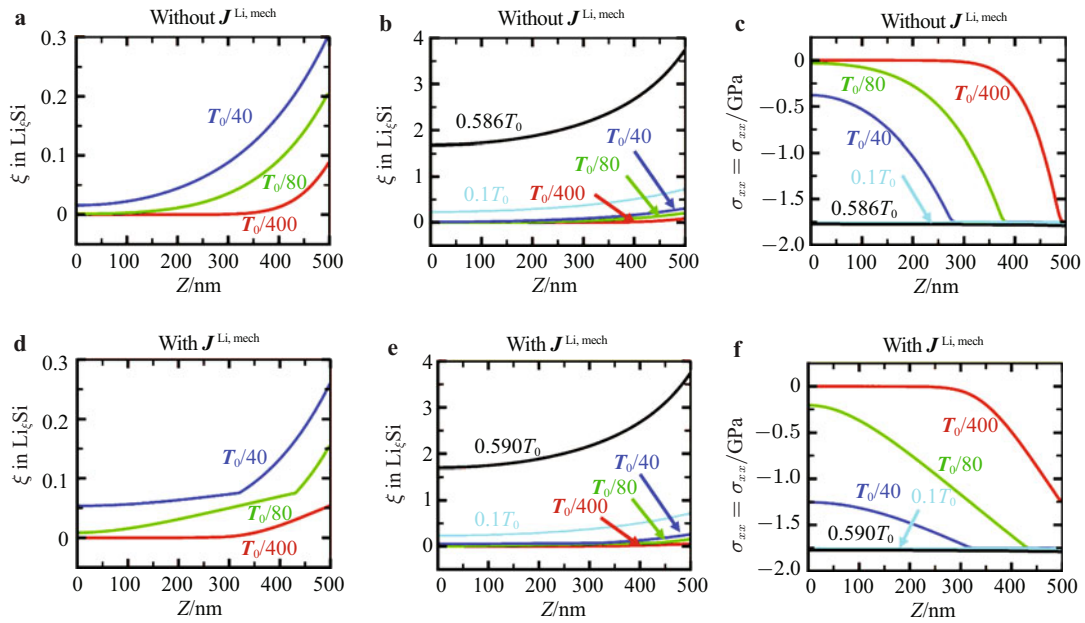

Fig. 4 **a, b, d, e** Normalized Li concentration and **c, f** stress profiles in a film with a thickness of $H = 500$ nm and fully constrained at the bottom (configuration in Fig. 1a). Here, lithiation-induced softening is not considered. **a-c** Normalized concentration and stress profiles without mechanical driving force for diffusion. **d-f** Normalized concentration and stress profiles with mechanical driving force for diffusion. For clarity, **a** and **d** show, with a finer vertical axis scale, the three early-stage profiles in **b** and **e**, respectively

On one hand, this deformation gradient is very different from that for the configuration in Fig. 1b (cf. Eq. (28)). On the other hand, the arguments on J_Z^{Li} drawn by Eqs. (21)–(26) are still valid. Indeed, Figs. 5a and 5b show similar J_Z^{Li} profiles as those in Fig. 3, at least to a first order of approximation. Although sharp kinks in J_Z^{Li} are seen in Fig. 5b for $t = T_0/80$ and $t = T_0/40$, the long-term profiles of J_Z^{Li} are fairly close to the 1st order approximation of $J_Z^{\text{Li}} \approx -ZJ_{\text{Surf}}^{\text{Li}}/H$. For reasons similar to those in Eqs. (28)–(30), the long-term Li concentration profiles are now governed by

$$\frac{\partial C^{\text{Li}}}{\partial Z} = C^{\text{Si}}\frac{\partial \xi}{\partial Z} \approx \frac{\left(J^{\text{SF}}\right)^2 ZJ_{\text{Surf}}^{\text{Li}}}{D_0^{\text{Li}}H}. \tag{34}$$

Here, because SED is lost when the film is under full scale yielding (i.e. $D^{\text{Li,eff}} = D_0^{\text{Li}}$), Eq. (34) is valid for both the situations with and without $\boldsymbol{J}^{\text{Li,mech}}$. A comparison of Eqs. (34) and (30) indicates that the long-term $\Delta\xi$ for Figs. 4b and 4e should be $\sim (J^{\text{SF}})^{4/3}$ times larger than $\Delta\xi$ in Fig. 2b. Simply speaking, because the current-configuration film thickness in the fully-constrained case is $(J^{\text{SF}})^{2/3}$ times larger than that in the partially-constrained case, Li must now traverse a longer distance, giving another reason for why the diffu-

sion is less efficient and $\bar{\xi}_{\text{end}}$ is smaller in Figs. 4b and 4e than in Fig. 2b. As discussed previously, the lower $\bar{\xi}_{\text{end}}$ in Figs. 4b and 4e compared to the $\bar{\xi}_{\text{end}}$ in Fig. 2b indicates that fully-constrained thin-film electrodes must be charged with a lower operational rate than their partially-constrained counterparts, if the same final state of charge $\bar{\xi}_{\text{end}}$ is required.

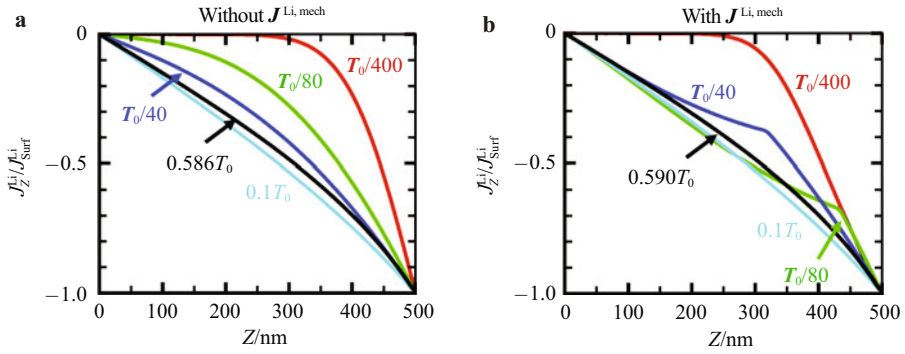

Fig. 5 Lagrangian lithium flux normalized by the surface influx when **a** mechanical driving force is not considered; **b** Mechanical driving force is considered. Z denotes Lagrangian coordinate. The film is fully constrained at the bottom and lithiation-induced softening is not considered

3.3 Stress-retarded diffusion due to plastic flow under lithiation-induced softening (configuration a)

It is important to note that diffusion in the fully-constrained film is slowed further when lithiation-induced softening is accounted for. To illustrate this effect, we first note that when $J_K^{\text{Li,mech}}$ is not considered (Figs. 6a and 6b), the concentration profiles are essentially the same as those in Figs. 4a and 4b, although the stresses (Fig. 6c) are significantly different from those in Fig. 4c. When the film undergoes full-scale yielding, the deformation gradients with and without lithiation-induced softening are comparable (both can be approximated by Eq. (33)). Therefore, in the absence of $J_K^{\text{Li,mech}}$, the two cases are governed by the same diffusion equations over approximately the same deformed configurations, hence, have roughly the same concentration profile. Indeed, $\bar{\xi}_{\text{end}}$ in Fig. 6b is approximately the same as that in Fig. 4b, and J_Z^{Li} in Fig. 7a is approximately the same as that in Fig. 5a.

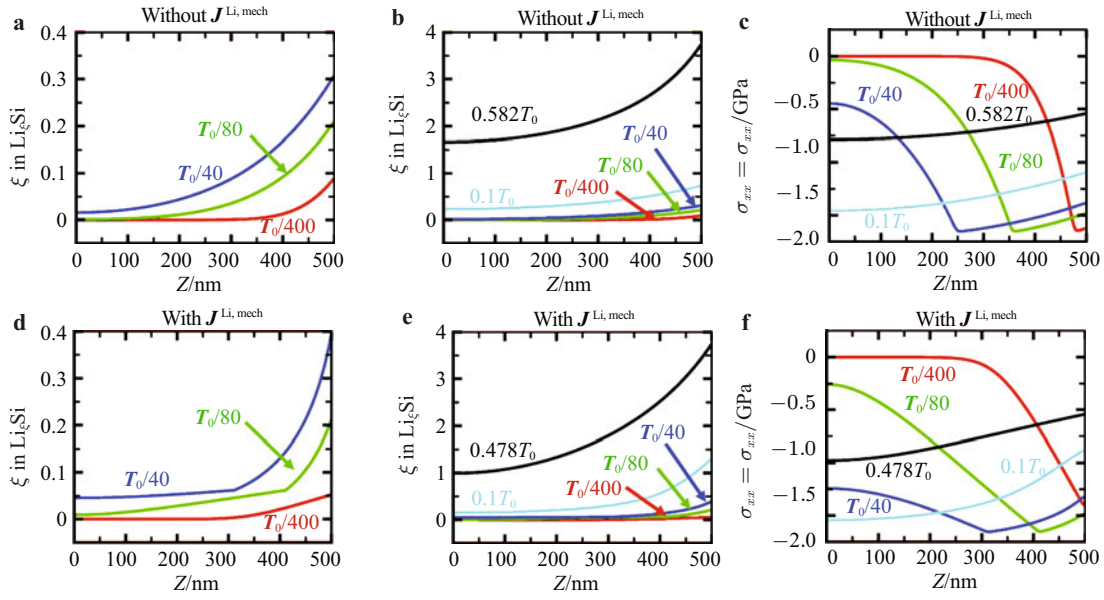

Fig. 6 **a, b, d, e** Normalized Li concentration and **c, f** stress profiles in a film with a thickness of $H = 500$ nm and constrained at the bottom (configuration in Fig. 1a). Lithiation-induced softening is considered. **a-c** Normalized concentration and stress profiles when the mechanical driving force for diffusion is not considered. **d-f** Normalized concentration and stress profiles when the mechanical driving force for diffusion is considered. For clarity, **a** and **d** show, with a finer vertical axis scale, the three early-stage profiles in **b** and **e**, respectively

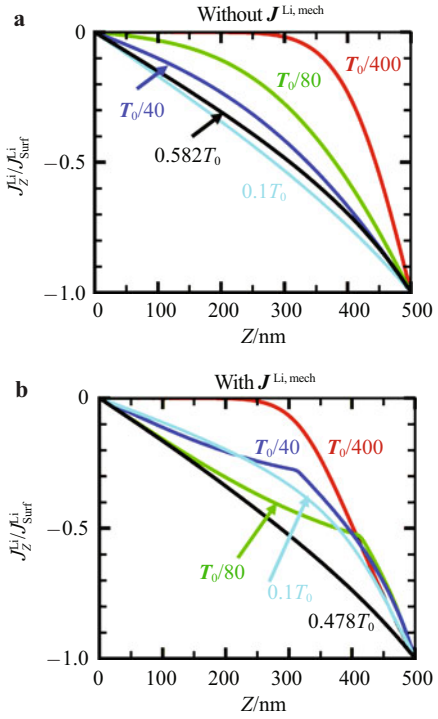

Fig. 7 Lagrangian lithium flux normalized by the surface influx when **a** mechanical driving force is not considered; **b** Mechanical driving force is considered. Z denotes Lagrangian coordinate. The film is fully constrained at the bottom and lithiation-induced softening is considered

However, when $J_K^{\text{Li,mech}}$ is considered, $\bar{\xi}_{\text{end}}^{\text{Li}}$ in Fig. 6e is $\sim$ 19% smaller than that in Fig. 4e and all the concentration profiles in Fig. 6e are significantly steeper than those in Fig. 4e. The reason lies in the fact that when composition-induced softening is considered, σ_{xx}, σ_{yy}, and hence σ_m are all smaller at the surface than at the center. Since $J_K^{\text{Li,mech}}$ always points towards the same direction as the gradient of σ_m, it contributes a driving force which tends to "squeeze" lithium upward toward the surface. Because such a driving force does not exist in the absence of lithiation-induced softening, diffusion is more efficient in Fig. 4 than in Fig. 6. Again, the 1st order approximation of Lagrangian flux profile is $J_Z^{\text{Li}} \approx -ZJ_{\text{Surf}}^{\text{Li}}/H$ (cf. Eqs. (21)–(26) and Fig. 7), i.e. the long-term profiles of J_Z^{Li} in Fig. 7 are not significantly different from those in Fig. 5, at least to a first order approximation. The less efficient diffusive transport therefore leads to steeper ξ profiles and hence lower $\bar{\xi}_{\text{end}}$ in Fig. 6 than in Fig. 4.

The retardation of diffusion due two-way coupling is in striking contrast to that seen in the elastic regime (Figs. 2d and 2e), in which stress effects always enhances diffusion. Indeed, the validity of Eq. (20) is strictly based on the premise that the deformation is elastic throughout the charging history. Our results indicate that whether the mechanical driving force assists or retards Li diffusion does not have a universal answer, and Li-transport is very sensitive to the externally applied mechanical constraints. This strong dependence of Li diffusion on mechanical constraints may help explain why Li diffusivities reported for different electrode configurations differ by several orders of magnitude, from 10^{-14} to 10^{-8} cm^{2}s^{-1} [13, 29–32], because it is the effective diffusivity $D^{\text{Li,eff}}$ instead of the tracer diffusivity D_0^{Li} that can be experimentally measured. Specifically, Ruffo et al. [31] measured $D^{\text{Li,eff}}$ for free-standing Si NWs to be 2×10^{-10} cm^2/s while Soni et al. [12] found that the upper bound for Li diffusivity in fully-constrained Si thin film is 10^{-11} cm^2/s. Using the ideal-solution assumption (Eqs. (16) and (20)), we estimate that the effective diffusivity $D^{\text{Li,eff}}$ during elastic deformation is ~20 times higher than D_0^{Li} for an intermediate state of charging of $\bar{\xi} = \xi_{\max}/2$. Such a $D^{\text{Li,eff}}$ is appropriate for free-standing Si NWs which is not subject to strong mechanical constraints. For Si thin films, in contrast, stresses retard instead of enhance diffusion, leading to an effective diffusivity $D^{\text{Li,eff}}$ that is on the order of or even lower than D_0^{Li}. The model in this paper is therefore consistent with the experimental findings by Ruffo et al. [31] and Soni et al. [11], in the sense that the $D^{\text{Li,eff}}$ may vary by one order of magnitude under different mechanical constraints. Admittedly, the ideal-solution assumption (Eq. (16)) in this paper entails a rather rough estimation of $\mu_{\text{SF}}^{\text{Li}}\left(C^{\text{Li}}\right)$. An accurate evaluation of $D^{\text{Li,eff}}/D_0^{\text{Li}}$ requires more realistic data on $\mu_{\text{SF}}^{\text{Li}}\left(C^{\text{Li}}\right)$ (which can be obtained once more accurate quasi-static OCP data is available). Such an evaluation is not the focus of this paper. Nevertheless, the main result, i.e., the strong dependence of diffusion on mechanical constraints, is not obscured by this uncertainty associated with $\mu_{\text{SF}}^{\text{Li}}\left(C^{\text{Li}}\right)$. At least, the analysis here indicates that the mechanical constraint is a very important factor to consider when interpreting experimentally measured diffusivities. While many other factors (such as deposition conditions for the amorphous Si) may affect the measured Li diffusivity, the analysis here indicates even the mechanical constraint alone can lead to variance in $D^{\text{Li,eff}}$ by one order of magnitude.

4 Conclusions

The finding that lithium diffusion is very sensitive to external constraint can have profound practical implications. The design of battery electrodes involves tradeoffs among capacity, cyclability and operational charging rate. The main advantage of alloy-based electrodes, especially Li/Si, is their much higher capacity compared with carbon-based electrodes. In terms of cyclability, it has been suggested that plastic flow can be beneficial for Li/Si electrodes because it relaxes stresses and thus reduces the chance of electrode failure. Our results here, however, indicate that there is another mechanism at work. On one hand, plasticity may help avoid electrode fracture – a mechanism that can be utilized by adopting measures that promote inelastic flow through the tailoring of material properties and changing charging/discharging regimen. On the other hand, plasticity may inhibit Li transport, especially under tight mechanical constraint. Under

any scenario, designs with less mechanical constraint on the electrodes are desirable because mechanical constraints diminishes stress-enhanced diffusion (SED) and magnifies the deleterious effect of plasticity and concentration-induced softening on Li transport. Because of these reasons, even in terms of operational charging rate alone, Li/Si nano-particles (e.g. nanospheres, nanoflakes, nanowires and nanotubes) are superior to Li/Si thin films or bulk materials. The results in this paper provide further support for nano-particles as building blocks for next-generation alloy-based electrodes.

Acknowledgement The project was supported by the National Research Foundation of Korea through WCU (R31-2009-000-10083-0).

References

1 Zhang, W. J.: A review of the electrochemical performance of alloy anodes for lithium-ion batteries. J. Power Sources **196**, 13–24 (2011)
2 Beaulieu, L. Y., Eberman, K. W., Turner, R. L., et al.: Colossal reversible volume changes in lithium alloys. Electrochem. Solid State Lett. **4**, A137–A140 (2001)
3 Christensen, J., Newman, J.: Stress generation and fracture in lithium insertion materials. J Solid State Electr. **10**, 293–319 (2006)
4 Chan, C. K., Peng, H. L., Liu, G., et al.: High-performance lithium battery anodes using silicon nanowires. Nature Nanotechnology **3**, 31–35 (2008)
5 Cui, L. F., Ruffo, R., Chan, C. K., et al.: Crystalline-amorphous core-shell silicon nanowires for high capacity and high current battery electrodes. Nano Letters **9**, 491–495 (2009)
6 Song, T., Xia, J. L., Lee, J. H., et al.: Arrays of sealed silicon nanotubes as anodes for lithium ion batteries. Nano Letters **10**, 1710–1716 (2010)
7 Magasinski, A., Dixon, P., Hertzberg, B., et al.: High-performance lithium-ion anodes using a hierarchical bottom-up approach. Nature Materials **9**, 353–358 (2010)
8 Hu, L., Wu, H., Gao, Y., et al.: Silicon-carbon nanotube coaxial sponge as li-ion anodes with high areal capacity. Advanced Energy Materials 523–527 (2011)
9 Kang, B., Ceder, G.: Battery materials for ultrafast charging and discharging. Nature. **458**, 190–193 (2009)
10 Bower, A., Guduru, P., Sethuraman, V.: A finite strain model of stress, diffusion, plastic flow, and electrochemical reactions in a lithium-ion half-cell. Journal of the Mechanics and Physics of Solids **59**, 804–828 (2011)
11 Zhao, K., Pharr, M., Cai, S., et al.: Large Plastic deformation in high-capacity lithium-ion batteries caused by charge and discharge. J Am Ceram Soc. **94**, S226–S235 (2011)
12 Soni, S., Sheldon, B., Xiao, X., et al.: Thickness effects on the lithiation of amorphous silicon thin films. Scripta Materialia. **64**, 307–310 (2011)
13 Johari, P., Qi, Y., Shenoy, V. B.: The mixing mechanism during lithiation of si negative electrode in li-ion batteries: an ab lnitio molecular dynamics study. Nano Lett. **11**, 5494–5500 (2011)
14 Bower, A. F., Guduru, P. R.: Asimple finite element model of diffusion, finited deformation, plasticity and fracture in lithium ion insertion electrode materials. Model Simul. Mater Sc. **20**, 045004 (2012)
15 Khan, A. S., Huang, S.: Continuum Theory of Plasticity, John Wiley & Sons, New York (1995).
16 Bower, A. F., Guduro, P. R., Sethuramana, V. A.: A finite strain model of stress, diffusion, plastic flow, and electrochemical reactions in a lithium-ion half-cell. Journal of the Mechanics and Physics of Solids **59**, 804 (2011)
17 Wu, C. H.: The role of Eshelby stress in composition-generated and stress-assisted diffusion. Journal of the Mechanics and Physics of Solids **49**, 1771–1794 (2001)
18 Larche, F., Cahn, J.: The interactions of composition and stress in crystalline solids. Acta Metallurgica. **33**, 331-357 (1985)
19 Purkayastha, R., Mcmeeking, R. M.: A linearized model for lithium ion batteries and maps for their performance and failure. Journal of Applied Mechanics **79**, 031032 (2012)
20 Yang, B., He, Y. P., Irsa, J., et al.: Effects of composition-dependent modulus, finite concentration and boundary constraint on Li-ion diffusion and stresses in a bilayer Cu-coated Si nano-anode. J. Power Sources **204**, 168–176 (2012)
21 Beaulieu, L. Y., Hatchard, T. D., Bonakdarpour, A., et al.: Reaction of Li with alloy thin films studied by in situ AFM. Journal of the Electrochemical Society **150**, A1457–A1464 (2003)
22 Gao, Y. F., Zhou, M.: Strong stress-enhanced diffusion in amorphous lithium alloy nanowire electrodes. Journal of Applied Physics **109**, 014310 (2011)
23 Shenoy, V., Johari, P., Qi, Y.: Elastic softening of amorphous and crystalline Li-Si Phases with increasing Li concentration: A first-principles study. J. Power Sources **195**, 6825–6830 (2010)
24 Chon, M., Sethuraman, V., Mccormick, A., et al.: Real-time measurement of stress and damage evolution during initial lithiation of crystalline silicon. Phys. Rev. Lett. **107**, 045503 (2011)
25 Sethuraman, V., Chon, M., Shimshak, M., et al.: In situ measurements of stress evolution in silicon thin films during electrochemical lithiation and delithiation. J. Power Sources **195**, 5062–5066 (2010)
26 Gao, Y., Zhou, M.: Strong stress-enhanced diffusion in amorphous lithium alloy nanowire electrodes. J. Appl. Phys. **109**, 014310 (2011)
27 Zhang, X., Shyy, W., Sastry, A.: Numerical simulation of intercalation-induced stress in Li-ion battery electrode particles. J. Electrochem Soc. **154**, A910–A916 (2007)
28 Ryu, I., Choi, J., Cui, Y., et al.: Size-dependent fracture of Si nanowire battery anodes. Journal of the Mechanics and Physics of Solids **59**, 1717–1730 (2011)
29 Ding, N., Xu, J., Yao, Y. X., et al.: Determination of the diffusion coefficient of lithium ions in nano-Si. Solid State Ionics **180**, 222–225 (2009)
30 Pell, E. M.: Diffusion of li in si at high-T and the isotope effect. Physical Review **119**, 1014–1021 (1960)
31 Ruffo, R., Hong, S. S., Chan, C. K., et al.: Impedance analysis of silicon nanowire lithium ion battery anodes. J. Phys. Chem. C **113**, 11390–11398 (2009)
32 Xie, J., Imanishi, N., Zhang, T., et al.: Li-ion diffusion in amorphous Si films prepared by RF magnetron sputtering: a comparison of using liquid and polymer electrolytes. Materials Chemistry and Physics **120**, 421–425 (2010)